An-Najah University Journal for Research – A
Natural Sciences

Kumada-Corriu Cross-Coupling Reaction Catalyzed by Cobalt Nanoparticles Arising from the Reductive Decomposition of a Cobaltacycle

Masoumeh Behzadi[1], Mélanie Boucher[1], Jérôme Robert[2] & Jean-Pierre Djukic[1,*]

(Type: Full Article). Received: 18th Jul. 2025, Accepted: 30th Aug. 2025, Published ××××, DOI: https://doi.org/10.xxxx

(This article belongs to the Special Issue: **Sustainable Materials and Chemistry for Energy and Environmental Applications**)

Accepted Manuscript, In press

Abstract: This study shows that the nanoparticles produced by the reductive decomposition of a cobalt (+III) metallacycle derived from 2-phenylpyridine upon treatment with the highly nucleophilic Na[Et_3BH] are capable of promoting the Kumada-Corriu cross coupling of aryl halides with aryl-bromomagnesium compounds (Grignard reagents) in various conditions and in the presence of various stabilizing ligands to afford the non-symmetric organic bisaryl product in reasonable yields. This study provides further evidence that incidental Co nanoparticles possess a reasonable capability in homogeneous catalysis, thereby complementing a prior report on their ability to promote the hydrosilylation of unsaturated organic substrates, such as nitriles. Co nanoparticles were characterized by HRTEM, EDX, EELS, and SAED techniques. TEM analyses revealed that the nanoparticles were uniformly spherical in shape, with a narrow size distribution; no nanoparticles larger than 3 nm were observed. EDX analysis displaying a characteristic Co signature at about 7 keV. The magnetic behavior of the nanoparticles studied by SQUID analysis in toluene using a temperature varied from 2 to 300 K, and a low magnetic field (10^{-3}T) in ZFC-FC conditions.

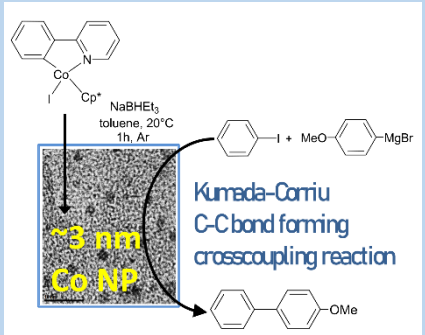

Keywords: Nanoparticle, Cobalt, Homogeneous catalysis, SQUID

Introduction

Current research trends that incite the development of innovative and sustainable catalysts based on earth-abundant 3d transition metals [1, 2] compel one to the imperative need for a complete understanding of the evolution of identified candidate catalysts during catalytic events. This exigency is not only required by the quest for sustainability with ecological, health, or ethical issues as preliminary criteria. It is also justified by the need to identify correctly the real "doers" of a given catalysis [3] to work on solid grounds to improve the performance of the said "actual active catalyst" and propose formulations with all implications being accounted for, including catalyst production, storage, use, recyclability, and disposal. Recent reports have shown that the chemistry of Co(III) organometallic or coordination complexes is multifaceted, falling well into problems that may have a tremendous impact on further developments at the industrial scale. It was shown that metallacyclic Co(III) complexes subjected to Oxidatively Induced Reductive Elimination (OIRE) conditions [4] may follow divergent pathways that are either productive or deleterious to the overall targeted catalytic process. [5] It was also shown[6] that spin state transitions, which are often overlooked, may unlock catalytic activity, allowing the emergence of a very promising alternative to both OIRE-based and photo-redox-induced catalysis of organic reactions by transition metals. The need to properly address the speciation of the catalyst by deliberately searching for a possible discrete but highly reactive nanoparticulate agent was stressed. [5] It was shown for instance that a class of Co(III) metallacycles can be used to promote hydrosilylation of various organic substrates if the said metallacycle is treated by a hydride source to produce a transient elusive hydrido intermediate that swiftly decomposes into Co-containing nanoparticles that were characterized by several adequate techniques [7]. In recent years, cobalt nanoparticles[8] have received important attention[9] due to their high potential in many fields of applications [10] and particularly in catalysis [11, 12]. A number of studies have already addressed methods to rationally engineer their morphology [13, 14] and therefore their physical and chemical properties [15-18]. The present study aimed at outlining that the adventitious nanoparticles formed by the reduction-induced decomposition of an organometallic complex, previously reported by us [7] , can promote in their native or slightly modified formulation a peculiar class of cross-coupling reactions, the Kumada-Corriu reaction,[19-21]. It is shown that the catalysis can slightly be improved by the use of additives such as potential nanoparticle (abbr. NP) outer surface ligands. Additional elements of characterization of the considered CoNP

1 Institute of Chemistry, UMR 7177 CNRS, University of Strasbourg, 4 rue Blaise Pascal, 67000 Strasbourg Cedex, France.
* Corresponding author email: djukic@unistra.fr
2 Department of Chemistry of Inorganic Materials (DCMI), IPCMS, 23 rue du Loess, 67037, Strasbourg Cedex 2, France.

by means of superconducting quantum interference device (SQUID) magnetometry is provided, which complement our previous [7] efforts of characterization of those incidental NP.

Materials and Methods

General: All experiments were conducted under a dry argon atmosphere using standard Schlenk lines and dry glovebox techniques. All glassware was oven-dried before use. All solvents were distilled over sodium or CaH2 under argon before use. Deuterated solvents were dried over sodium or CaH2, filtered over activated neutral alumina, and stored under argon before use. Compounds [CoCp*(2-phpy)I] 3, 5-chloro-benzo[h]quinoline, and 5-bromo-benzo[h]quinoline were prepared according to literature procedures [22, 23]. The following compounds were purchased from Sigma-Aldrich: sodium triethylborohydride solution (Na[BHEt3], 1 M in toluene), phenylmagnesiumbromide solution (PhMgBr, 1 M in tetrahydrofuran – abbr. THF -), 4-methoxyphenylmagnesiumbromide solution (abbr. MeOPhMgBr, 0.5 M in THF), n-hexylmagnesiumbromide solution (abbr. hexMgBr, 2 M, in THF), isopropylmagnesiumbromide solution (i-PrMgBr, 0.75 M in THF), 4-tert-butylphenylmagnesium bromide solution (abbr. 4-t-BuPhMgBr, 3.0 M in diethyl ether), 4-fluorophenylmagnesiumbromide solution (abbr. 4-F-PhMgBr 1.0 M in THF), bromobenzene (99%), 3-bromoanisole (98%), 4-Bromoanisole (99%), 2-bromotoluene (99%),3-bromotoluene (98%), 4-bromotoluene (98%), 2-bromoaniline (98%), 3-bromoaniline (98%), 4-bromoaniline (97%), 1-bromo-2-nitrobenzene (98%), 1-bromo-4-nitrobenzene (99%), iodobenzene (98%), 1-iodo-2-nitrobenzene (97%), 1-iodo-4-nitrobenzene (98%), chlorobenzene (99.5%), 2-chlorotoluene (99%), 4-chlorotoluene (98%) and N,N-bismesityl-imidazolidinylidene [24]. 1H (300, 400, 500, and 600 MHz) and 13C (75 and 126 MHz) NMR spectra were measured on Bruker DPX 300 and 400, Avance I 500 spectrometers. Chemical shifts (δ) are expressed in parts per million (ppm) and are referenced against solvent peaks or external reference standards (Me4Si in CDCl3 for 1H and 13C). Mass spectra were run on a MicroTOF Bruker Daltonics spectrometer, using a TOF-ESI coupling analysis system. 1H NMR yields were calculated by comparing the integration of a product of interest against an internal reference introduced in known amount (namely 1,3,5-tri-tert-butylbenzene). Whenever the products of the catalysis were already reported, their identity and purity were assessed by NMR and referred to the original report in the literature.

Typical conditions of TEM, EDS, EELS, and SQUID analyses: TEM studies were performed either using a parallel incident electron beam (TEM mode) or an electron probe scanned on the sample (STEM mode). The UTEM (Ultrafast TEM), a JEOL 2100, operating at 200 kV, is equipped with a thermionic gun, two mirror systems, and an extra electron lens. The optical tables, which house the lasers and delay lines, are coupled to the column, allowing the entire system to be compact and supported by the microscope's anti-vibration system. A femtosecond laser (370 fs) and two nanosecond lasers (7 ns) are used. The microscope is also equipped with an electron energy-loss spectrometer (Gatan Enfinium). The FEG-TEM 2100F, TEM with a field effect gun and owning better resolution in TEM and STEM mode, operating at 200 kV, allowing a 0.16 nm resolution in STEM, and 0.12 nm in TEM mode. It is equipped with a high brightness electron source and highly efficient EDS detectors, which make it ideally suited for fast elemental mapping at the sub-nanometer scale. The EELS spectrometer is a GIF TRIDIEM, with a 1 eV resolution, and the data were acquired in TEM mode. It must be noted that samples deposited on the copper grids were shortly exposed to air, causing partial incorporation of O in the EDS and EELS signatures. A superconducting quantum interference device (SQUID) magnetometer was used to measure the magnetic properties of cobalt nanoparticles: the magnetic analysis was carried out using a SQUID VSM magnetometer (Quantum Design) on a sample consisting of a homogenous solution of the CoNP in toluene contained in a air-tight teflon sample tube, which was prepared in an Ar-filled glove box to prevent any uncontrolled oxidation during the preparation and the measure. Temperature was varied from 2 to 300 K, and 10-3 T magnetic fields was applied.

Synthesis of [Cp*CoI2]2 [23]. [Co2(CO)8] (1958 mg, 5.73 mmol) and 1,2,3,4,5-pentamethylcyclopentadiene (Cp*H) (2 mL, 12.8 mmol, 2.2 equiv.) were refluxed at 55°C in CH2Cl2 (20 mL) for 4 h and left overnight under stirring at 37°C. The solvents were evaporated to dryness. The dark red [CoCp*(CO)2] was dissolved in Et2O (20 mL) and added to a solution of I2 (2.9 g, 11.42 mmol) in Et2O (50 mL). After stirring at room temperature for about 1 h, the precipitate was separated from the supernatant by filtration and washed with Et2O. The red solution was dried under vacuum to produce a dark red solid, which was purified by column chromatography (silica, pentane to 4:1 CH2Cl2: pentane). After drying, the pure dark red solid was isolated. The obtained [Cp*CoI2(CO)] (1414 mg, 2.97 mmol) was refluxed in heptane (150 mL) for 3 days at 120 °C to generate [Cp*CoI2]2. After purification by column chromatography (silica, eluent gradient from pentane to CH2Cl2: MeOH), the product was isolated as a dark green solid (yield: 20%). 1H NMR (300 MHz, CDCl3, δ): 1.80 (s, 30H).

Synthesis of LiNHAc [23]. Acetamide (945 mg, 15.9 mmol) was dissolved in 20 mL of THF in a sealed Schlenk vessel under an Ar atmosphere, and the resulting solution was cooled to −80 °C. The resulting solution was vigorously stirred and then added with a solution of n-BuLi in hexane (1.6 M, 1 equiv., 10 mL). The resulting suspension was left to react overnight while the vessel was slowly warmed to room temperature. The resulting suspension was then filtered, and the collected solid was washed with dry n-pentane and dried under reduced pressure (77% yield). IR (ATR, neat): □□ 1588 (m, C=O stretching) cm−1. 1H NMR (400 MHz, CDCl3) δ 7.26 (d, J = 1.6 Hz, 1H), 2.01 (s, 3H).

Synthesis of Iodo (pentamethylcyclopentadienyl)(2-phenylenepyridine-κ^2-C,N) cobalt(III) [23]. Under an argon atmosphere, a mixture of $[Cp^*CoI_2]_2$ (448 mg, 0.5 mmol, 1 equiv.), LiNHAc (195.1 mg, 3 mmol, 6 equiv.), and 2-phenylpyridine (143 µL, 1 mmol, 2 equiv.) were stirred in 10 mL of CH_2Cl_2 at 50 °C for 48 h in a sealed Schlenk vessel. The reaction mixture was filtered through Celite, followed by removal of the solvent. The resulting residue was then purified by recrystallization with CH_2Cl_2/*n*-pentane and washing with *n*-pentane to afford **3** as a dark green solid in 74% yield. ^{1}H NMR (300 MHz, $CDCl_3$) δ 9.20 (d, *J* = 5.7 Hz, 1H), 8.27 (d, *J* = 7.7 Hz, 1H), 7.62 (dd, *J* = 5.0, 2.0 Hz, 2H), 7.59 – 7.46 (m, 1H), 7.29 (d, *J* = 7.4 Hz, 1H), 7.04 (dd, *J* = 8.4, 6.1 Hz, 2H), 1.49 (s, 15H); ^{13}C NMR (126 MHz, $CDCl_3$) δ 181.4, 167.2, 155.0, 145.7,142.5, 136.6, 129.4, 123.3, 122.7, 121.2, 118.5, 93.5, 10.4. The analytical data matched those reported by us previously [23].

Procedure for the synthesis of Cobalt nanoparticles CoNP: [Cp*CoI(2-*phpy*)] (4 mg, 0.0084 mmol) was treated with $Na[BHEt_3]$ (0.168 mL, 0.0168 mmol, 0.1 M in toluene, 2 equiv.) in 2 mL toluene at 20°C. After 1h stirring under argon atmosphere, the black green solution was filtered over Celite and diluted 10 times with dry degassed toluene to produce a clear solution suitable for transmission electron microscopy (TEM), electron energy loss spectroscopy (EELS), energy-dispersive X-ray spectroscopy (EDX), selected area electron diffraction (SAED), and superconducting quantum interference device (SQUID) magnetometry analyses.

Solubility and Persistence Assessment for CoNP: the dark-green solutions of CoNP, octylamine@CoNP, and NHC@CoNP were filtered through Celite, resulting in clear filtrates, which were stored in a glove box under argon at room temperature for three weeks. These clear solutions remained stable over an extended period, showing neither precipitation nor aggregation for octylamine@CoNP and NHC@CoNP. For CoNP, only a negligible metallic deposit formed with a slight solution color change. Additionally, the catalytic reactivity of the NHC@CoNP solution was evaluated (Eq. 1) with iodobenzene, and the yield in cross-coupling remained unchanged as compared to a reference run carried out with a freshly prepared solution of CoNP. Furthermore, dark-green solutions of CoNP were centrifuged at 10000 rpm for 10 minutes at 25°C. The clear solution and the black solid portion were separated under an argon atmosphere, then added to a tenfold amount of dry and degassed toluene, and analyzed by TEM. TEM showed nanoparticles with a uniformly spherical shape and an average size of 2–2.5 nm in the solution, while no CoNPs were observed in the solid phase.

Synthesis of CoNP Stabilized by Arduengo's Mes_2-Im Heterocyclic Carbene, abbr. NHC: [Cp*CoI(2-phpy)] (4 mg, 0.0084 mmol) reacted with Na[BHEt3] (0.168 mL, 0.0168 mmol, 0.1 M in toluene, 2 equiv.) in 2 mL toluene at 20°C. After 1h stirring under Argon, a solution of 0.5 mg 1,3-bis(mesityl)-2-imidazolidinylidene (0.0017 mmol, [NHC]/[Co], 0.2 equiv.) in 0.2 mL toluene, which was prepared in the glove box, was added to the mixture and was allowed to stir at room temperature for 2 hours. This black green solution was filtered over Celite and diluted 10 times with toluene to create a clear and homogeneous solution for SQUID analysis.

Synthesis of CoNP Stabilized by *n*-octylamine: [Cp*CoI(2-phpy)] (4 mg, 0.0084 mmol) was reacted with Na[BHEt3] (0.168 mL, 0.0168 mmol, 0.1 M in toluene, 2 equiv.) in 2 mL of toluene at 20°C. After 1 hour of stirring under argon, octylamine (0.0017 mmol, [NHC]:[Co]=0.2:1 equiv., 28 µL) was added to the mixture and stirred at room temperature for 15 hours. The black-green solution was filtered over Celite and had to be diluted 10 times with toluene to produce a clear solution suitable for SQUID analysis.

General Procedure for the syntheses of ligands 5-Chloro-benzo[*h*]quinoline *and* 5-Bromo-benzo[*h*]quinoline (2). Under aerobic conditions, benzo[h]quinoline (5 g, 27.9 mmol) was added portion-wise to a reaction flask containing 45 mL of vigorously stirred concentrated sulfuric acid (95–98 %), at room temperature. After cooling, N-bromosuccinimide (abbr. NBS, 4.96 g, 27.87 mmol) or N-chlorosuccinimide (abbr. NBS, 3.75 g, 27.7 mmol) was slowly added to maintain the temperature inside the flask below 35°C, and the resulting reaction mixture was stirred overnight. The mixture was slowly poured into 250 mL of ice-cold water and subsequently carefully neutralized with a saturated ammonia solution to pH~6. The precipitated product was extracted with chloroform and the resulting organic phase washed with water thrice. The resulting organic layer was dried over anhydrous magnesium sulfate, filtered and concentrated in vacuum to give the crude product as a yellowish oil. Flash chromatography using n-pentane/diethyl ether (15:1, v/v) afforded a new oily residue, which upon recrystallization from boiling diethyl ether, produced a white solid (60%).

Coupling Reaction of Arylmagnesium Bromides with Aryl Halides, General Procedure: Under argon, aryl halides (0.168 mmol, one equiv.), the Grignard reagent (0.252 mmol, 1.5 equiv.) was added sequentially via a syringe to the in situ-prepared solution of CoNP, NHC@CoNP, and octylamine@CoNP(5 mol%) at a slow rate. After stirring at 25°C for four hours, the solvent was removed under reduced pressure, and the product was recovered by flash-silica gel column chromatography using a dichloromethane/pentane mixture (1/3) as eluent.

Results and Discussion

Co-NP complementary characterizations characterization

In our previous report [7] on the formation of Co nanoparticles from the reductive decomposition of a cobaltacycle, it was found that the most optimal conditions for their formation required the treatment of the organometallic complex with a minimum of 2 equiv. of Na[BHEt3] in toluene at room temperature. TEM analysis under aerobic conditions revealed that this procedure yields NPs with an average diameter of 2.5 nm. In the present study, the same method was used, and TEM analyses carried out under identical conditions confirmed the reproducibility of the small-sized NPs generation. Further characterizations, such as EELS and EDX, produced signatures similar to those reported previously, and the SAED applied to a liquid sample of CoNPs revealed a feature of crystallinity of the analyzed NPs, but was not able to characterize it further. The missing magnetic information was acquired by the SQUID magnetometry on the neat sample of CoNP but also on the samples resulting from its treatment with supposedly stabilizing ligands,[15, 25, 26], namely octylamine and the room temperature-stable so-called Arduengo's N,N-bis-mesityl-imidazolidinylidene [27] that were added in a 0.2:1 molar ratio with respect to the expected Co content, which seems to be an optimal compromise according to Valero et al. [27].

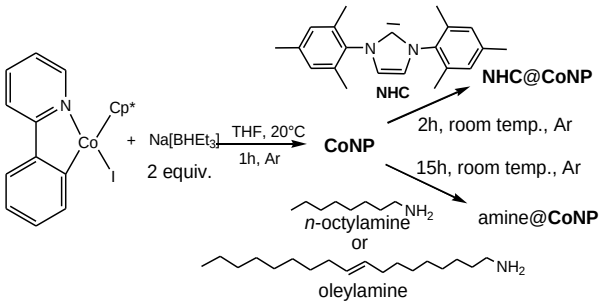

Scheme (1): Preparation of **CoNP** and its treatment with stabilizing ligands.

ZFC-FC results on the neat *in vitro* made CoNP. A temperature-dependent magnetization measurement was carried out from 2 to 300 K under a low magnetic field (10-3T) in both zero-field-cooled (ZFC) and field-cooled (FC) conditions. The ZFC and FC magnetization curves do not fully overlap

across the entire temperature range, indicating the presence of multiple magnetic phases in the CoNP solution. A noticeable difference between the ZFC and FC curves appears at low temperatures (5–100 K), while the curves start to converge above 100 K and fully overlap around 200 K, marking the Curie temperature (TC), where the transition from ferromagnetic to paramagnetic behavior occurs. At 300 K, a small residual magnetization remains, suggesting persistent ferromagnetism. A narrow peak in the ZFC curve is observed at 5 K (blocking temperature, TB). The difference between FC and ZFC magnetization decreases with increasing temperature and is nearly zero at room temperature, further confirming the multiphase nature of the sample.

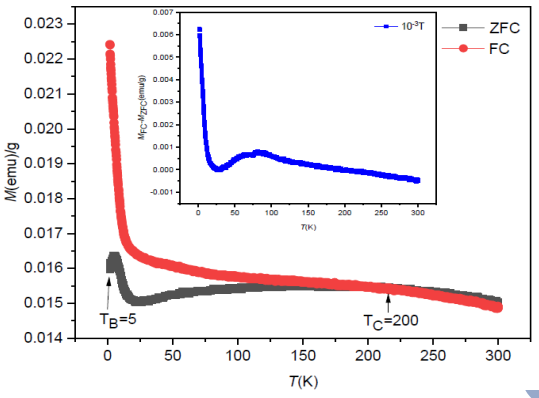

Figure (1): ZFC and FC magnetization versus temperature at 10^{-3} T magnetic field for **CoNP** solution in toluene, where TB = 5 k and TC = 200 K. Inset shows the difference between the FC and ZFC magnetization (ΔM) against temperature.

Hysteresis curve of the neat CoNP. The hysteresis curve is an essential aspect in studying the magnetization of CoNP. It offers insights into key magnetic properties such as saturation magnetization (Ms), coercivity (Hc), and remanence (Mr). The shape of the hysteresis loop indicates the magnetic behavior of ferromagnetic nanomaterials [28-30].

The values of saturation magnetization (Ms) and remanent magnetization (Mr) at 5 K are 1.135 and 0.13 emu/g, respectively. While the Ms and Mr values are moderate, the coercivity (Hc) at 5 K is relatively high at 306 Oe, especially when compared to the values of Ms and Mr.

At 300 K, the values of saturation magnetization (Ms) and remanent magnetization (Mr) are 0.27 and 0.033 emu/g, respectively. Although the coercivity values at 300 K and 5 K differ significantly, the ratio of remanent to saturation magnetization (Mr/Ms) remains nearly the same—0.12 at 300 K and 0.115 at 5 K. This suggests that a similar magnetic field is required to reverse the magnetization at both temperatures.

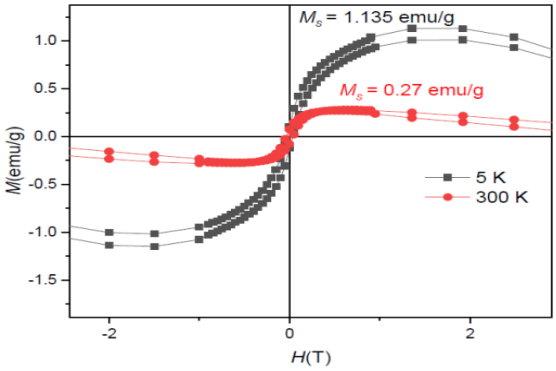

Figure (2): Field-dependent magnetization measurement, hysteresis loop, for a solution of cobalt nanoparticles in toluene measured at 5 K and 300 K respectively.

Magnetic properties of CoNPs stabilized by ligands [16, 28]**.** The SQUID results indicate that ligand stabilization of NPs slightly reduces the saturation magnetization and may shift the blocking temperature. However, it still maintains the essential superparamagnetic behavior, indicating successful surface modification without affecting the core magnetic properties.

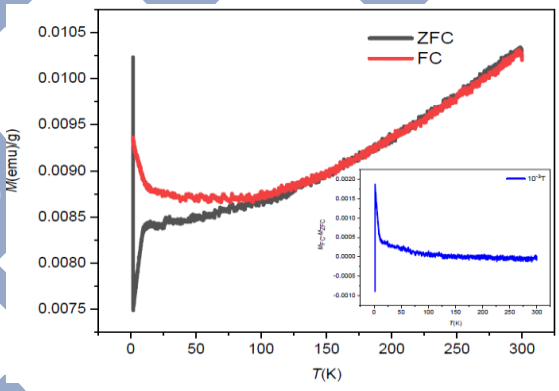

Figure (3): ZFC and FC magnetization versus temperature at 10^{-3} T magnetic field for octylamine@**CoNP** solution in toluene, where T_B = 40-50 k and T_C is above 300 K. Inset shows the difference between the FC and ZFC magnetization (ΔM) against temperature.

ZFC-FC Analysis of octylamine@CoNP at 10^{-3}T. The ZFC and FC magnetization versus temperature curves, measured under an applied magnetic field of 10^{-3} T between 2 and 300 K, are shown in Figure 3. A comparison of the ZFC and FC curves shows that magnetization (M) increases steadily with temperature. Although there is no sharp divergence between the ZFC and FC curves, a clear separation is observed. A broad maximum in the ZFC curve around 40–50 K indicates that the blocking temperature (TB) likely falls within this range. The broad peak in the ZFC curve, along with its divergence from the FC curve, suggests superparamagnetic behavior, with the nanoparticles in a blocked state below 50 K and transitioning to a superparamagnetic state above this temperature.

Effect of amine binding. The low magnetization values (0.009–0.0105 emu/g) indicate a diluted magnetic response, likely due to surface spin disorder from amine ligands, reduced core volume, and increased inter-particle distance, which weakens dipolar interactions. Amine binding slightly suppresses overall magnetization but preserves superparamagnetic behavior. For octylamine@**CoNP**, no clear Curie temperature (T_C) is observed, as the material exhibits superparamagnetism rather than bulk ferromagnetism. In such systems, the blocking temperature (T_B) is more relevant, with T_C typically much higher.

The magnetization plot up to 300 K shows no abrupt drop, further supporting the absence of a T_C transition.

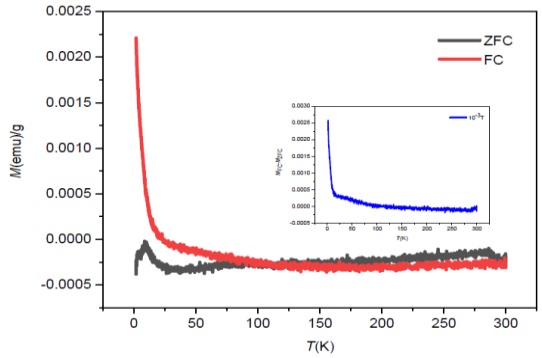

Figure (4): ZFC and FC magnetization versus temperature at 10^{-3} T magnetic field for NHC@**CoNP** solution in toluene where T_B = 60 K and T_C is above 300 K. Inset shows the difference between the FC and ZFC magnetization (ΔM) against temperature.

NHC@CoNP at 10^{-3} T. A clear separation between ZFC and FC curves appears below 60 K. This temperature can be interpreted as the blocking temperature (T_B) 60 K, and indicates superparamagnetism below T_B. Above 150 K, both ZFC and FC magnetization values are close to zero and converge, indicating paramagnetic behavior. This suggests a low concentration of magnetic material or strong surface and ligand effects suppressing net magnetization—typical of functionalized superparamagnetic nanoparticles. NHC ligands, which form strong covalent bonds with metal surfaces, can disrupt spin alignment, induce spin canting[29] or disorder, and reduce inter-particle magnetic coupling. Furthermore, this superparamagnetism with a very weak magnetic response is probably due to small particle size (strong surface effects), well-stabilized by NHC ligands that minimize aggregation and interactions.

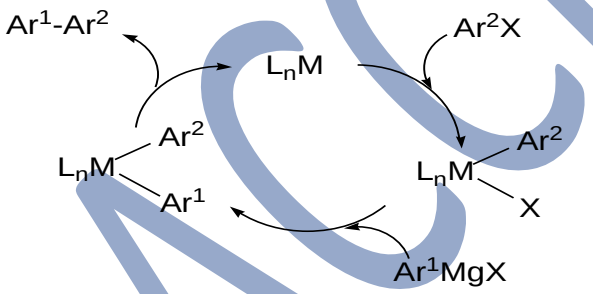

Scheme (2): Kumada-Corriu cross-coupling reaction starting from a low-valent metal catalyst.

Kumada-Corriu crosscoupling reaction promoted by neat CoNP and ligand-stabilized nanoparticles, *i.e.* ligand@CoNP

The Kumada-Corriu reaction[19, 20] is a C-C bond-forming cross-coupling reaction between a Grignard reagent and an alkyl or aryl halide that was systematically studied for its mechanism in the 1970s and has witnessed a wide range of applications in organic synthesis[30]. Its generic mechanism entails the oxidative addition of the halogenated substrate on a low-valent metal center of a molecular coordination complex, followed by an arylation of the metal center by the Grignard reagent in a transmetallation step gathering around the metal center the two organic moieties. The latter two are subsequently eliminated in a reductive elimination step that produces the organic product of interest and regenerates the metal center in its lower valence state ready for the next catalytic cycle. The substrates targeted here in this reactivity benchmark of the **CoNP** are essentially iodo, bromo and chloro arenes, the latter representing a sort of challenge due to the lower capability of the C_{Ar}-Cl bond to undergo the oxydative addition on a metal centre.

Table (1): The reaction of ArMgBr with ArX in the presence of **CoNP** in THF.

Entry	Grignard	Aryl halide	Time (h)	*T* (℃)	Yield (%)
1	4-MeO-PhMgBr	PhI	4	25	74
2	4-MeO-PhMgBr	PhBr	4	25	66
3	4-MeO-PhMgBr	PhCl	15	50	56
4	PhMgBr	4-bromoanisole	4	25	60
5	PhMgBr	4-chloroanisole	4	25	54
6	4-F-PhMgBr	PhI	4	25	8
7	4-F-PhMgBr	PhI	15	25	14
8	*n*-C_6H_{13}MgBr	PhI	15	25	0

Conditions: Aryl halides (0.168 mmol, 1 equiv), **CoNP** (5 mol%, 4 mg), and Grignard reagents (0.252 mmol, 1.5 equiv) in THF (2 mL); 1,3,5-tri-tert-butylbenzene, and 1,3,5-trimethoxybenzene as internal ^{1}H NMR standard.

To identify the optimal conditions, we evaluated a prototypical system of reagents (iodobenzene and 4-methoxyphenylmagnesiumbromide + **CoNP**) for the optimal temperature and solvent conditions to achieve the highest yield in the bis-aryl cross-coupling reaction product. The supporting Information lists those various conditions and shows that the best yield (74%) in hetero-cross-coupling product is obtained in 4 h at 25°C when tetrahydrofuran is used as the co-solvent (remember that toluene is used to form **CoNP**, giving rise to a stock solution used in all catalysis runs). The use of dichloromethane (DCM) or toluene drastically decreases the performance of the catalysis. At 25°C, in dichloromethane (DCM), the yield barely reaches 50% in 24 h. At the same time, toluene limits the yield to a maximum of 33% in 4h, and any prolongation of the reaction time does not improve significantly (24h of reaction only produces the product in 37% yield). Table 1 lists the performance of the **CoNP** catalyst with various Grignard reagents and shows that the attempted reaction of the aliphatic *n*-C_6H_{13}MgBr with PhI did not yield any product. In turn, all the aryl Grignard reagents performed with a net sensitivity to the presence of the electron-withdrawing substituent F- in 4-fluorophenylmagnesiumbromide, which hardly achieves with PhI the heterocross-coupling reaction in 14% yield.

The catalyst's ability to perform the cross-coupling reaction with bromo- and chlorobenzene and -anisole is quite impressive, achieving yields of over 50% at either 25°C (entry 5, Table 1) or 50°C (entry 3, Table 1). Table 2 shows the performance of CoNP with 4-methoxyphenylmagnesiumbromide as the Grignard reagent on a broader range of aryl iodide, bromide and chlorides (Equ. 1). For aryl iodides and bromides, the yields are nearly all above 50% within four hours of reaction time, except for 5-bromobenzo[h]quinoline, which requires a longer reaction time to reach 54% yield.

The efficiency of the C-C coupling reaction strongly depends on both the type of halogen (I > Br > Cl) (Table 2, entries 1, 4, 20) and the substitution pattern (electronic and steric effects). Electron-withdrawing substituents (e.g., $-NO_2$) on the aryl halide enhance the electrophilicity of the C-X bond and tend to enhance

the oxidative addition, especially when located para to the halogen. For example, a $–NO_2$ group at the para position of phenyl iodide increases the reaction yield from 74% to 87% (Table 2, entries 1-2). Deactivation by the electron-withdrawing substituent –CF3 is moderate and does not preclude catalysis. With aryl chlorides, a temperature of 50°C and long reaction times >10 h are required to achieve yields above 50%, except in the case of 2-chlorotoluene, which remains stuck at around 12% yield after 15h of reaction.

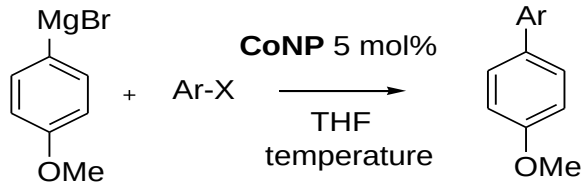

Equation (1)

Table (2): Cobalt NP-catalyzed Kumada-Corriu coupling reactions of aryl halides with 4 methoxyphenylmagnesium bromide with CoNP(~5 mol%) in THF.

Entry	X	Ar-X	Time (h)	T (°C)	yield (%)	ref.
1	I	PhI	4	25	74	[31]
2	I	1-iodo-4-nitrobenzene	4	25	87	[31]
3	I	1-iodo-2-nitrobenzene	4	25	53	[31]
4	Br	bromobenzene	4	25	66	[32]
5	Br	4-bromoanisole	4	25	87	[31]
6	Br	3-bromoanisole	4	25	50	[33]
7	Br	4-bromotoluene	4	25	73	[31]
8	Br	3-bromotoluene	4	25	69	[31]
9	Br	2-bromotoluene	4	25	66	[31]
10	Br	1-bromo-4-nitrobenzene	4	25	53	[31]
11	Br	1-bromo-2-nitrobenzene	4	25	48	[31]
12	Br	4-bromoaniline	4	25	62	[31]
13	Br	2-bromoaniline	4	25	52	[31]
14	Br	5-bromobenzo[h]quinoline	4	25	26	[22]
15	Br	5-bromobenzo[h]quinoline	15	25	54	[22]
16	Br	4-bromotrifluoromethylbenzene	4	25	57	[31]
17	Br	3-bromotrifluoromethylbenzene	4	25	54	[34]
18	Br	2-bromotrifluoromethylbenzene	4	25	52	[34]
19	Br	2-bromopyridine	15	50	81	[31]
20	Cl	chlorobenzene	15	50	55	[31]
21	Cl	4-chlorotoluene	15	50	60	[31]
22	Cl	2-chlorotoluene	15	50	21	[31]
23	Cl	5-chlorobenzo[h]quinoline	4	50	12	[22]
24	Cl	5-chlorobenzo[h]quinoline	15	50	51	[22]

Bulky groups near the halogen at the ortho position can hinder the oxidative addition step and thus lower reactivity. Conversely, para-substituents mainly affect reactivity through electronic effects (Table 2, entries 1–3). Meta-substituents exert weaker effects because of their low electronic conjugation to the reaction site. As shown in Table 2 (entries 7–9), placing a moderately bulky group like methyl at different positions on the aryl halide follows a logical trend: steric hindrance at the ortho position reduces the yield more significantly than at the para or meta positions.

Table (3): Ligand-stabilized **CoNP** evaluation for Kumada coupling reactions of aryl halides with 4-methoxyphenylmagnesiumbromide in THF.

Entry	Catalyst	X	Ar-X	Time (h)	*T* (°C)	Yield (%)
1	**CoNP**	I	PhI	4	25	74
2	**NHC@CoNP**	I	PhI	4	25	84
3	octylamine@**CoNP**	I	PhI	4	25	73
4	oleylamine@**CoNP**	I	PhI	4	25	47
5	**CoNP**	Br	PhBr	4	25	66
6	**NHC@CoNP**	Br	PhBr	4	25	84
7	**CoNP**	Cl	PhCl	15	25	11
8	**CoNP**	Cl	PhCl	15	50	55
9	**NHC@CoNP**	Cl	PhCl	4	25	48

All yields were determined against an internal NMR reference (1,3,5-tri-tert-butylbenzene).

The use of auxiliary ligands was considered to evaluate their effect on the performance of the catalysis. Such ligands are generally expected to bind the surface of the nanoparticles and protect them from various processes that are deleterious to their integrity, such as aggregation and oxidation. However, it was shown that the amount of ligand had to be also controlled to avoid the aggregation of ligand-bound NPs by lipophilic forces. In this study, three ligands available from commercial sources were used, namely n-octylamine, oleylamine, and Arduengo's [24] N-heterocyclic N,N- bis-mesitylimidazolidinylidene.

Table 3 shows how these ligands affect catalytic performance. While n-octylamine added in small amounts [15] does not significantly change the catalysis performance (entry 3, Table 3) compared to the initial CoNP case, oleylamine appears to be somewhat harmful (entry 4, Table 3). The NHC ligand, in contrast, slightly improves the catalysis, allowing it to reach 84% yield (entry 2, Table 3) for the coupling of 4-methoxyphenylmagnesiumbromide with iodobenzene. For chlorobenzene, the most notable result is that NHC@CoNP (entry 9, Table 3) increases the yield of the hetero cross-coupling with 4-methoxyphenylmagnesiumbromide by 30% at 25°C.

Finally, cycling the same catalytic pot on the prototypical coupling of iodobenzene with 4-methoxyphenylmagnesium bromide using the native CoNP and the NHC@CoNP could be done for about 3-4 cycles without reducing the yield of the cross-coupling product, the yield dropping by 10% at the fifth cycle.

Conclusion

This study confirms that the incidental spherical CoNP of small size fromed by the reductive decomposition of a cobaltacycle bears a significant capability to promote the Kumada - Corriu reaction with arene substrates. These results add another catalytic virtue to this class of cobalt nanoparticles. Their ability to promote two different reactions deserve to investigate deeper their chemical properties in the presence of stabilizing ligands. This study identified the potential of Arduengo's stable alkylidene, which improved the catalytic performance with chlorobenzene which constitutes a promising ground for further developments. SQUID magnetometry carried out under anaerobic conditions (i.e., argon protective atmosphere) further confirms the ferro/paramagnetic properties of the nanoparticles arising from the hydride-initiated decomposition of the 2-phenylpyridine bonded Cp*-bonded cobaltacycle. Further efforts shall be put at characterizing **CoNP** under anaerobic condition and evaluate *in operando* techniques

for the investigation of **CoNP** modification during the course of a catalyzed reaction.

- **Ethics approval and consent to participate:** Not applicable.
- **Consent for publication:** Not applicable
- **Availability of data and materials:** The raw data required to reproduce these findings are available in the body and illustrations of this manuscript and in the supporting information.
- **Author's contribution:** The authors confirm their contributions to the paper as follows: study conception and design by Behzadi, magnetometry by Robert, and data analysis and validation by Behzadi and Djukic. draft manuscript preparation: Behzadi, Djukic. All authors reviewed the results and approved the final version of the manuscript.
- **Funding:** CNRS, University of Strasbourg, IDEX Attractivity, Program PAUSE.
- **Conflicts of interest:** The authors declare that there is no conflict of interest regarding the publication of this article.
- **Acknowledgements:** The authors are particularly grateful to the program PAUSE and the IDEX funding of the University of Strasbourg for covering the hosting of M.B in our laboratory.

Open Access

References

1] Kaplaneris N, Ackermann L. Earth-abundant 3d transition metals on the rise in catalysis. Beil J Org Chem. 2022;18:86-8.

2] Gandeepan P, Müller T, Zell D, Cera G, Warratz S, Ackermann L. 3d Transition Metals for C–H Activation. Chem Rev. 2019;119(4):2192-452.

3] García-Viada A, Carretero JC, Adrio J, Rodríguez N. Insights into the mechanism of 3d transition-metal-catalyzed directed C(sp3)–H bond functionalization reactions. Chem Soc Rev. 2025;54(9):4353-90.

4] Antuña-Hörlein C, Djukic J-P. Unlocking Catalysis Using Oxidatively Induced Reductive Elimination. Chem – Eur J. 2025;31(18):e202404341.

5] Wu F, Deraedt C, Cornaton Y, Ruhlmann L, Karmazin L, Bailly C, Kyritsakas N, Le Breton N, Choua S, Djukic J-P. Fate of Cobaltacycles in Cp*Co-Mediated C–H Bond Functionalization Catalysis: Cobaltacycles May Collapse upon Oxidation via Co(IV) Species. Organometallics. 2021;40(15):2624-42.

6] Wang Z, Cornaton Y, Djukic J-P. Triplet State-Promoted Kumada-Corriu Coupling Catalyzed by Hydrotris(3,5-diisopropylpyrazolyl)boratocobalt(III)diiodide. Eur J Inorg Chem. 2024;27(34):e202400420.

7] Antuña-Hörlein C, Wu F, Deraedt C, Bouillet C, Djukic J-P. Cobalt Nanoparticles Formed upon Reaction of Cp*Co(III) Metallacycles with Na[BHEt3] Show Catalytic Activity in the Hydrosilylation of Aryl Ketones, Aldehydes and Nitriles. Eur J Inorg Chem. 2023;26(6):e202200563.

8] Margeat O, Amiens C, Chaudret B, Lecante P, Benfield RE. Chemical Control of Structural and Magnetic Properties of Cobalt Nanoparticles. Chem Mater. 2005;17(1):107-11.

9] Frey NA, Peng S, Cheng K, Sun S. Magnetic nanoparticles: synthesis, functionalization, and applications in bioimaging and magnetic energy storage. Chem Soc Rev. 2009;38(9):2532-42.

10] Khusnuriyalova AF, Caporali M, Hey-Hawkins E, Sinyashin OG, Yakhvarov DG. Preparation of Cobalt Nanoparticles. Eur J Inorg Chem. 2021;2021(30):3023-47.

11] Chng LL, Erathodiyil N, Ying JY. Nanostructured Catalysts for Organic Transformations. Acc Chem Res. 2013;46(8):1825-37.

12] Yi D, Min Y, Muzzi B, Marty A, Romana I, Fazzini P-F, Blon T, Viau G, Serp P, Soulantica K. Epsilon Cobalt Nanoparticles as Highly Performant Catalysts in Cinnamaldehyde Selective Hydrogenation. ACS Appl Nano Mater. 2022;5(4):5498-507.

13] Li Y, Liu Q, Shen W. Morphology-dependent nanocatalysis: metal particles. Dalton Trans. 2011;40(22):5811-26.

14] Schällibaum J, Dalla Torre FH, Caseri WR, Löffler JF. Large-scale synthesis of defined cobalt nanoparticles and magnetic metal–polymer composites. Nanoscale. 2009;1(3):374-81.

15] Vivien A, Guillaumont M, Meziane L, Salzemann C, Aubert C, Halbert S, Gérard H, Petit M, Petit C. Role of Oleylamine Revisited: An Original Disproportionation Route to Monodispersed Cobalt and Nickel Nanocrystals. Chem Mater. 2019;31(3):960-8.

16] Meziane L, Salzemann C, Aubert C, Gérard H, Petit C, Petit M. Hcp cobalt nanocrystals with high magnetic anisotropy prepared by easy one-pot synthesis. Nanoscale. 2016;8(44):18640-5.

17] Dobbrow C, Schmidt AM. Improvement of the oxidation stability of cobalt nanoparticles. Beilstein J Nanotechnol. 2012;3:75-81.

18] Bergmann A, Roldan Cuenya B. Operando Insights into Nanoparticle Transformations during Catalysis. ACS Catalysis. 2019;9(11):10020-43.

19] Tamao K, Sumitani K, Kumada M. Selective carbon-carbon bond formation by cross-coupling of Grignard reagents with organic halides. Catalysis by nickel-phosphine complexes. J Am Chem Soc. 1972;94(12):4374-6.

20] Corriu RJP, Masse JP. Activation of Grignard reagents by transition-metal complexes. A new and simple synthesis of trans-stilbenes and polyphenyls. J Chem Soc, Chem Commun. 1972(3):144a-a.

21] Kharasch MS, Fields EK. Factors Determining the Course and Mechanisms of Grignard Reactions. IV. The Effect of Metallic Halides on the Reaction of Aryl Grignard Reagents and Organic Halides1. J Am Chem Soc. 1941;63(9):2316-20.

22] Behzadi M, Gajendramurthy CM, Boucher M, Deraedt C, Cornaton Y, Karmazin L, Gruber N, Bertani P, Djukic J-P. Electrophilic Si−H Activation by Acetonitrilo Benzo[h]quinoline Iridacycles: Influence of Electronic Effects in Catalysis. Chem – Eur J. 2023;29(43):e202300811.

23] Wu F, Deraedt C, Cornaton Y, Contreras-Garcia J, Boucher M, Karmazin L, Bailly C, Djukic J-P. Making Base-Assisted C–H Bond Activation by Cp*Co(III) Effective: A Noncovalent Interaction-Inclusive Theoretical Insight and Experimental Validation. Organometallics. 2020;39(14):2609-29.

24] Arduengo AJ, III, Dias HVR, Harlow RL, Kline M. Electronic stabilization of nucleophilic carbenes. J Am Chem Soc. 1992;114(14):5530-4.

25] Pan C, Pelzer K, Philippot K, Chaudret B, Dassenoy F, Lecante P, Casanove M-J. Ligand-Stabilized Ruthenium Nanoparticles: Synthesis, Organization, and Dynamics. J Am Chem Soc. 2001;123(31):7584-93.

26] Bao Y, An W, Turner CH, Krishnan KM. The Critical Role of Surfactants in the Growth of Cobalt Nanoparticles. Langmuir. 2010;26(1):478-83.

27] Valero M, Bouzouita D, Palazzolo A, Atzrodt J, Dugave C, Tricard S, Feuillastre S, Pieters G, Chaudret B, Derdau V. NHC-Stabilized Iridium Nanoparticles as Catalysts in Hydrogen Isotope Exchange Reactions of Anilines. Angew Chem Int Ed. 2020;59(9):3517-22.

28] Osuna J, de Caro D, Amiens C, Chaudret B, Snoeck E, Respaud M, Broto J-M, Fert A. Synthesis, Characterization, and Magnetic Properties of Cobalt Nanoparticles from an Organometallic Precursor. J Phys Chem. 1996;100(35):14571-4.

29] Ngo AT, Bonville P, Pileni MP. Spin canting and size effects in nanoparticles of nonstoichiometric cobalt ferrite. J Appl Phys. 2001;89(6):3370-6.

30] Heravi MM, Zadsirjan V, Hajiabbasi P, Hamidi H. Advances in Kumada–Tamao–Corriu cross-coupling reaction: an update. Monatsh Chem. 2019;150(4):535-91.

31] Mao S-L, Sun Y, Yu G-A, Zhao C, Han Z-J, Yuan J, Zhu X, Yang Q, Liu S-H. A highly active catalytic system for Suzuki–Miyaura cross-coupling reactions of aryl and heteroaryl chlorides in water. Org Biomol Chem. 2012;10(47):9410-7.

32] Tabatabaei Rezaei SJ, Shamseddin A, Ramazani A, Mashhadi Malekzadeh A, Azimzadeh Asiabi P. Palladium nanoparticles immobilized on amphiphilic and hyperbranched polymer-functionalized magnetic nanoparticles: An efficient semi-heterogeneous catalyst for Heck reaction. Appl Organomet Chem. 2017;31(9):e3707.

33] Li D-H, He X-X, Xu C, Huang F-D, Liu N, Shen D-S, Liu F-S. N-Heterocarbene Palladium Complexes with Dianisole Backbones: Synthesis, Structure, and Catalysis. Organometallics. 2019;38(12):2539-52.

34] Xu L-Y, Liu C-Y, Liu S-Y, Ren Z-G, Young DJ, Lang J-P. Suzuki-Miyaura cross-coupling reaction of aryl chlorides with aryl boronic acids catalyzed by a palladium dichloride adduct of N-diphenylphosphanyl-2-aminopyridine. Tetrahedron. 2017;73(22):3125-32.